Chapter 5

Non-Stoichiometry in $A_2B_2O_7$ Pyrochlores

> *"So he thinks that they hold on to one another and remain together up to the time when some stronger force reaches them from their environment and shakes them and scatters them apart."*
>
> *- Aristotle*
>
> *On Democritus, c.350 BC*

5.1 Introduction

Due to the extensive compositional range of the compounds which exhibit the pyrochlore structure, there are a variety of actual and potential applications for these materials. Examples include: dielectric materials [199, 200], catalysts [201, 202], solid electrolytes [203–205], thermal barrier coatings [206, 207] as well as actinide host phases for nuclear waste encapsulation [208–211]. Given this broad range of functionality, in order to tailor pyrochlore properties it is desirable to understand their non-stoichiometry in a consistent manner.

Here, the $A_2B_2O_7$ pyrochlores in which A is strictly a 3+ cation and B a 4+ cation are considered (refer to Chapter 1 for a detailed description of pyrochlore crystallography). Our aim is to predict the mechanisms that accommodate non-stoichiometry and thereby provide data that can be evaluated against A_2O_3-BO_2 binary phase diagrams. As such, 4+ cations are not allowed to exhibit variable charge states, despite the fact that cations such as Ti, Ru, Mo and Pb are able to exhibit a 3+ charge state. If 3+ charge states were included for the B cations, the appropriate comparison would be to ternary A_2O_3-BO_2-B_2O_3 phase diagrams, none of which have been found in the literature (although ternary phase diagrams do exist for certain A_2O_3-BO_2-$A\prime_2O_3$ combinations, such as HfO_2 - Y_2O_3 - Er_2O_3 and HfO_2 - Y_2O_3 - La_2O_3 [212, 213]). Similarly, the possibility that Pr^{3+} may be oxidized to a 4+ charge state is not considered (Note: Ce^{3+} and Tb^{3+} may also exhibit a 4+ charge state although these cations are not explicitly modelled).

5.1.1 Review of Phase Diagrams

Existing experimental work relating to non-stoichiometry has focused exclusively on determining phase diagrams. Of the pyrochlores modelled explicitly in this study, there exist selected phase diagrams that include compounds in the series $A_2Ti_2O_7$ and $A_2Zr_2O_7$. The titanate pyrochlores $Lu_2Ti_2O_7$, $Yb_2Ti_2O_7$, $Dy_2Ti_2O_7$, $Sm_2Ti_2O_7$, $Nd_2Ti_2O_7$ and $La_2Ti_2O_7$ exhibit stability in the form of a line compound [214–218]. In all of the corresponding phase diagrams, pyrochlores are reported between 900^o - 2000^oC, see for example Figure 5.1.

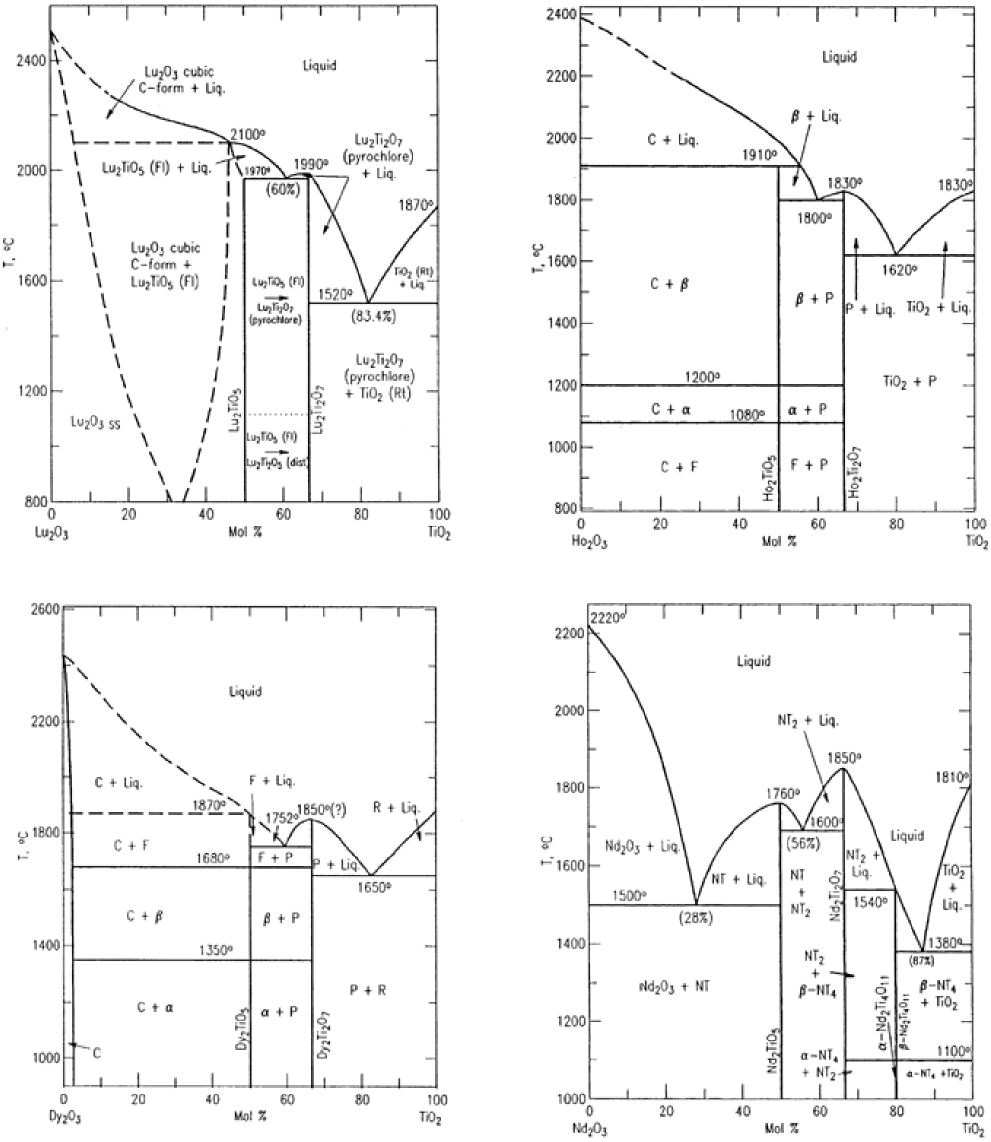

Figure 5.1: Phase diagrams of the $A_2Ti_2O_7$ series of compounds for small A^{3+} cations, reproduced from [214, 215, 217].

However, there exist several other titanate phase diagrams (e.g. $Dy_2Ti_2O_7$, $Er_2Ti_2O_7$, $Sm_2Ti_2O_7$ and $Y_2Ti_2O_7$ [219–222]) which demonstrate modest non-stoichiometry. An example of this is shown in Figure 5.2, where there is an extended pyrochlore phase field in the Y_2O_3 -TiO_2 system. The dashed line between the fluorite and pyrochlore phase regions is an undetermined boundary, as the investigators were unable to establish the two phase region.

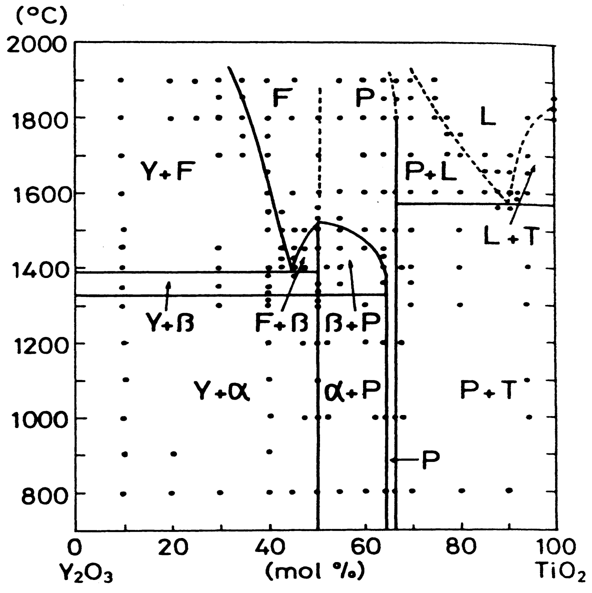

Figure 5.2: The phase diagram of the Y_2O_3 -TiO_2 system, reproduced from [222].

An interesting comparison of phase diagrams is provided by two in the Sm_2O_3 - TiO_2 system, shown in Figure 5.3. Clearly, there are glaring differences between these two phase diagrams, especially in the region of the pyrochlore phase. Such inconsistency in the titanate series of phase diagrams does not lend itself to quantitative comparison with our calculations, though the qualitative information is useful.

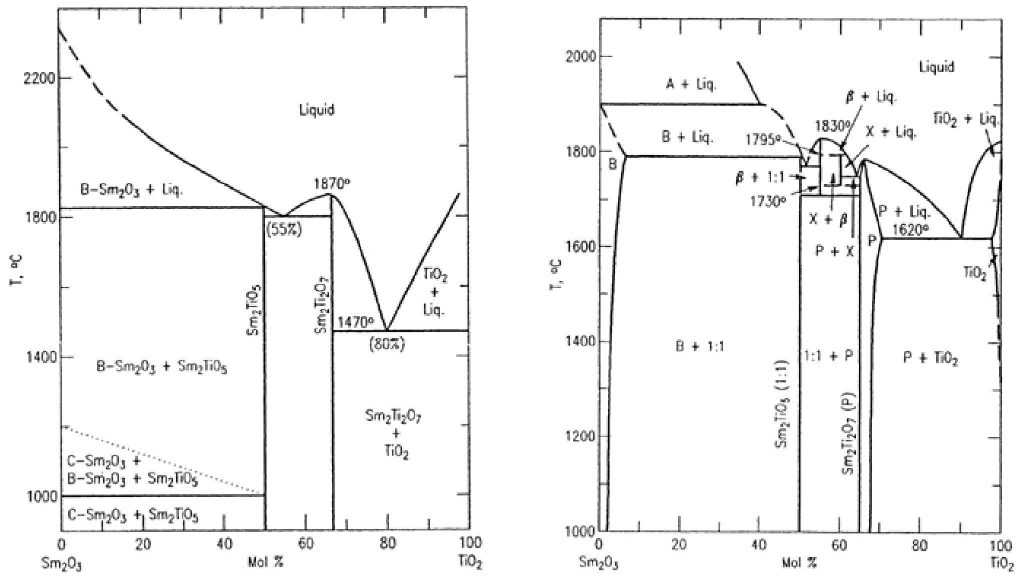

Figure 5.3: Comparison of Sm_2O_3 - TiO_2 phase diagrams, where the pyrochlore phase in the left diagram is a line compound while in the right hand diagram exhibits modest non-stoichiometry; reproduced from [216] and [221], respectively.

There are several potentially pertinent phase diagrams within the zirconate series. However, in those diagrams the pyrochlore phase regime is usually extrapolated. Figure 5.4 depicts such hypothetical pyrochlore phase regions for $Eu_2Zr_2O_7$, $Gd_2Zr_2O_7$ and $Sm_2Zr_2O_7$ [223–225]. Furthermore, the bottom two phase diagrams in Figure 5.4 both describe the Sm_2O_3 - ZrO_2 system, albeit differently. Nevertheless, these diagrams suggest that zirconates will exhibit both BO_2 and A_2O_3 non-stoichiometry.

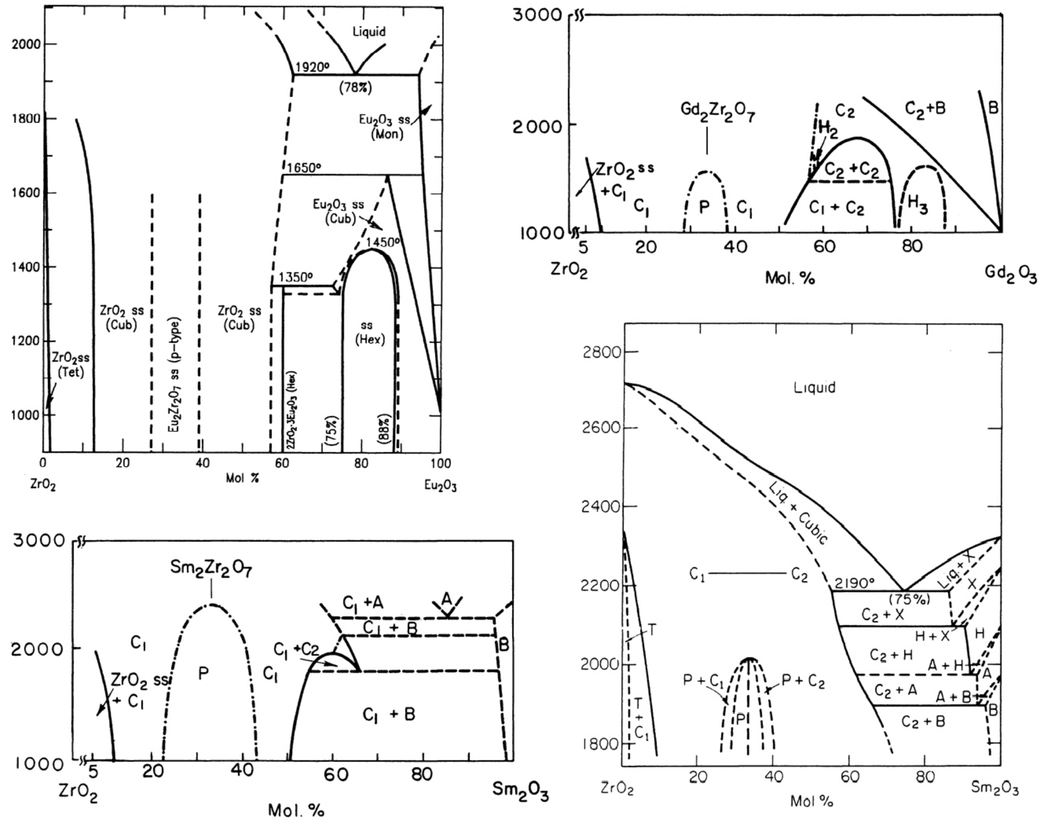

Figure 5.4: Comparison of Eu_2O_3 - ZrO_2, Gd_2O_3 - ZrO_2 and Sm_2O_3 - ZrO_2 phase diagrams, where the pyrochlore region in each diagram is hypothesized; reproduced from [223–225].

A singular exception from the hypothesized pyrochlore phase region is in the La_2O_3 - ZrO_2 system [224, 225], in which the pyrochlore regime is well defined, see the top two phase diagrams in Figure 5.5. However, substantial differences exist between these two reported La_2O_3 - ZrO_2 phase diagrams. These two diagrams can be compared to three phase diagrams of the same system, shown in the bottom of Figure 5.5. Although the three diagrams display probable phase regions, when compared to the two phase diagrams above, it is clear that this system is not very well understood.

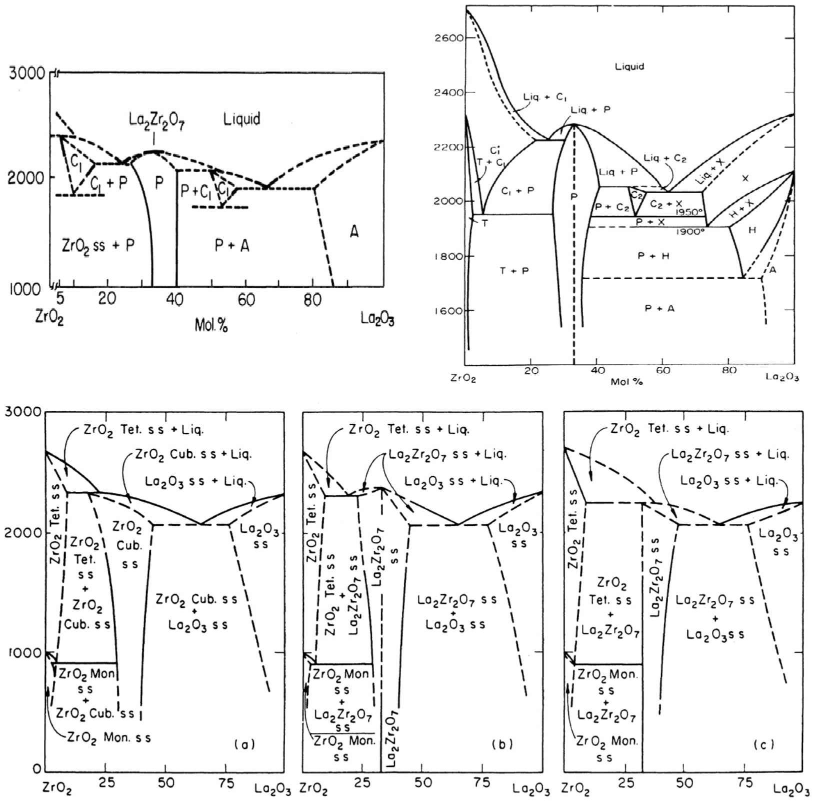

Figure 5.5: Several La_2O_3 - ZrO_2 phase diagrams, reproduced from [224], [225] and [226, 227] respectively.

Returning to the zirconate phase diagrams with hypothesized pyrochlore regimes, for example the two describing the Nd_2O_3 - ZrO_2 series [225–227], there exist substantial differences, see Figure 5.6. Again, it is difficult to quantitatively compare our calculated results to these phase diagrams. However, what can be qualitatively noted from the zirconate series, when compared to the titanate series, is the increased extent of pyrochlore non-stoichiometry.

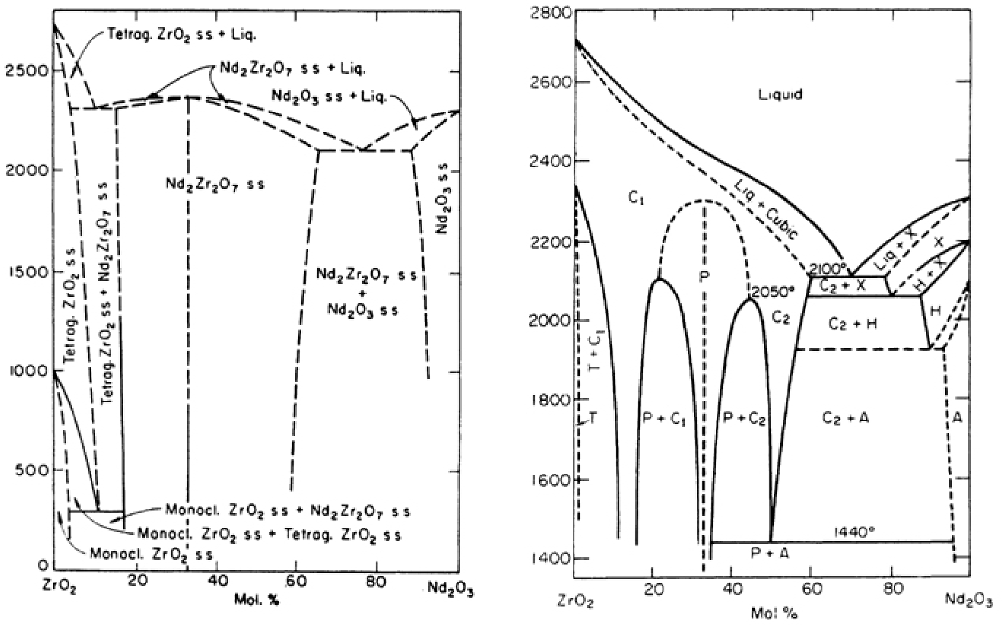

Figure 5.6: Comparison of Nd_2O_3 - ZrO_2 phase diagrams, reproduced from [226, 227] and [225] respectively.

There have been recent theoretical calculations of zirconate phase diagrams. Figure 5.7 depicts phase diagrams for the Y_2O_3 - ZrO_2 and La_2O_3 - ZrO_2 systems as calculated by Yokokawa *et al.* [228]. It is interesting to compare these two phase diagrams to those generated through experiment. The diagram on the right depicting the La_2O_3 - ZrO_2 system can be compared to Figure 5.5. In both the experimental and theoretical diagrams, a pyrochlore phase clearly exists. However, in the experimentally generated diagrams, there is pronounced non-stoichiometry, while for the theoretical, the pyrochlore phase appears only as a line compound.

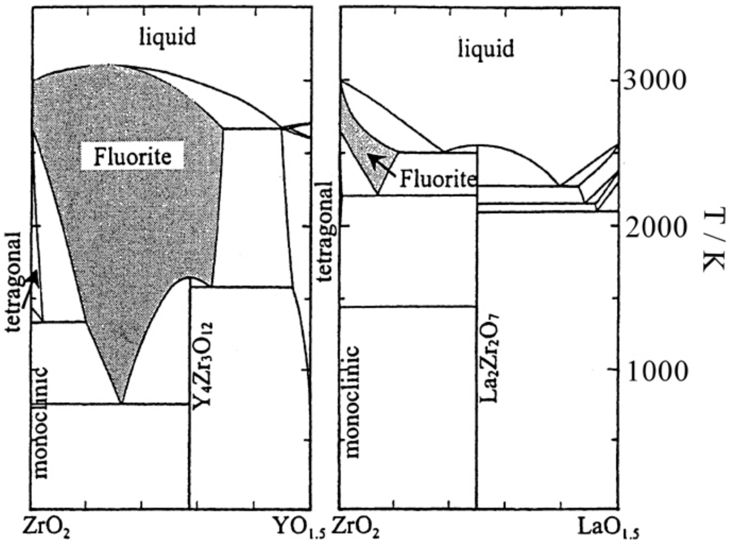

Figure 5.7: ZrO_2 - A_2O_3 phase diagrams calculated by Yokokawa *et al.* [228].

The left diagram in Figure 5.7 depicts the Y_2O_3 - ZrO_2 system. Due to the technological significance of this system, there has been considerable experimental effort in order to generate the phase diagram. Figure 5.8 displays a representative evolution of this phase diagram, reproduced from various sources [229–234]. The details of these phase diagrams are not pertinent here and can be found in the original texts, but it should be noted that in both the theoretical and experimental phase diagrams for the Y_2O_3 - ZrO_2 system, there is no indication of a $Y_2Zr_2O_7$ pyrochlore phase, although a $Y_4Zr_3O_{12}$ phase is reported.

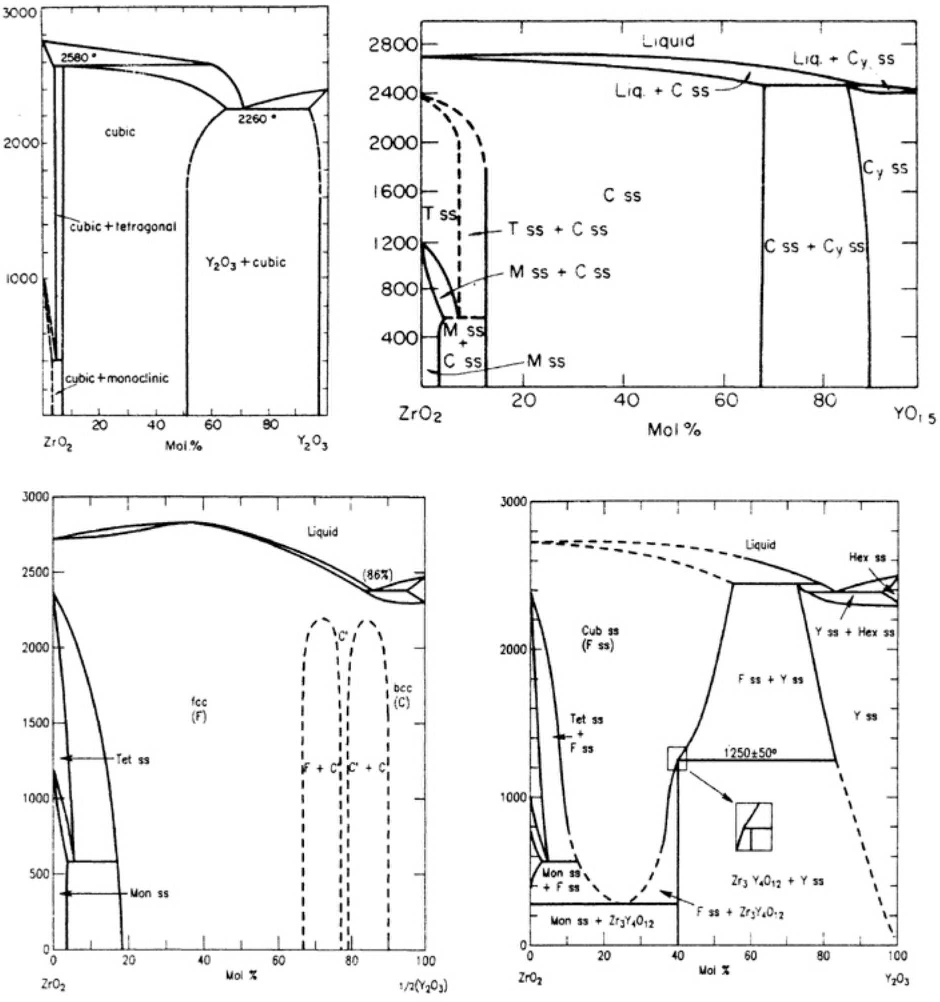

Figure 5.8: Experimental phase diagrams of the Y_2O_3 - ZrO_2 system, reproduced from [229] and [230] respectively for the top two diagrams and [231,232] and [233,234] respectively for the bottom two diagrams.

A more complete set of phase diagrams exists for the $A_2Hf_2O_7$ series of compounds, with pyrochlore phases reported between 1600^o - 2500^oC. Although hafnium has not been explicitly modelled, zirconium and tin were considered explicitly, and their ionic radii, 0.72Å and 0.69Å respectively [6], lie either side of hafnium, 0.71Å. Thus, the computational data for hafnium can be extrapolated and subsequently can be compared to experimental data [235–238]. The hafnate phase diagrams show that the pyrochlore structure is stable from La^{3+} (1.16Å) to Tb^{3+} (1.04Å), but with no pyrochlore phase field apparent for the smaller A^{3+} cations from Dy^{3+} (1.027Å) to Lu^{3+} (0.977Å), see Figures 5.9 and 5.10.

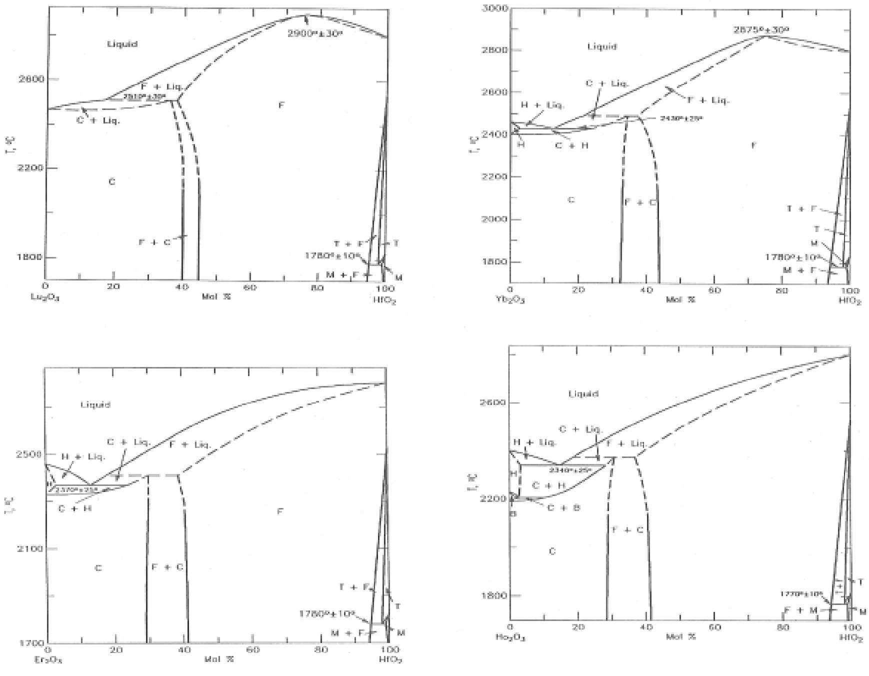

Figure 5.9: Phase diagrams of the $A_2Hf_2O_7$ series of compounds for small A^{3+}, reproduced from [235]. Here the A^{3+} cations have the ionic radii of $Lu^{3+} = 0.977$Å, $Yb^{3+} = 0.985$Å, $Er^{3+} = 1.004$Å and $Ho^{3+} = 1.015$Å.

The transition from the non-existence of a pyrochlore phase to the emergence of such a phase is depicted in Figure 5.10, with the Dy_2O_3 - HfO_2 system displaying no pyrochlore phase, while Tb_2O_3, Gd_2O_3 and Sm_2O_3 - HfO_2 do exhibit a pyrochlore phase. This transition will be revisited in Chapter 6. For now, the dependence of pyrochlore stability on A^{3+} cation radius is simply noted.

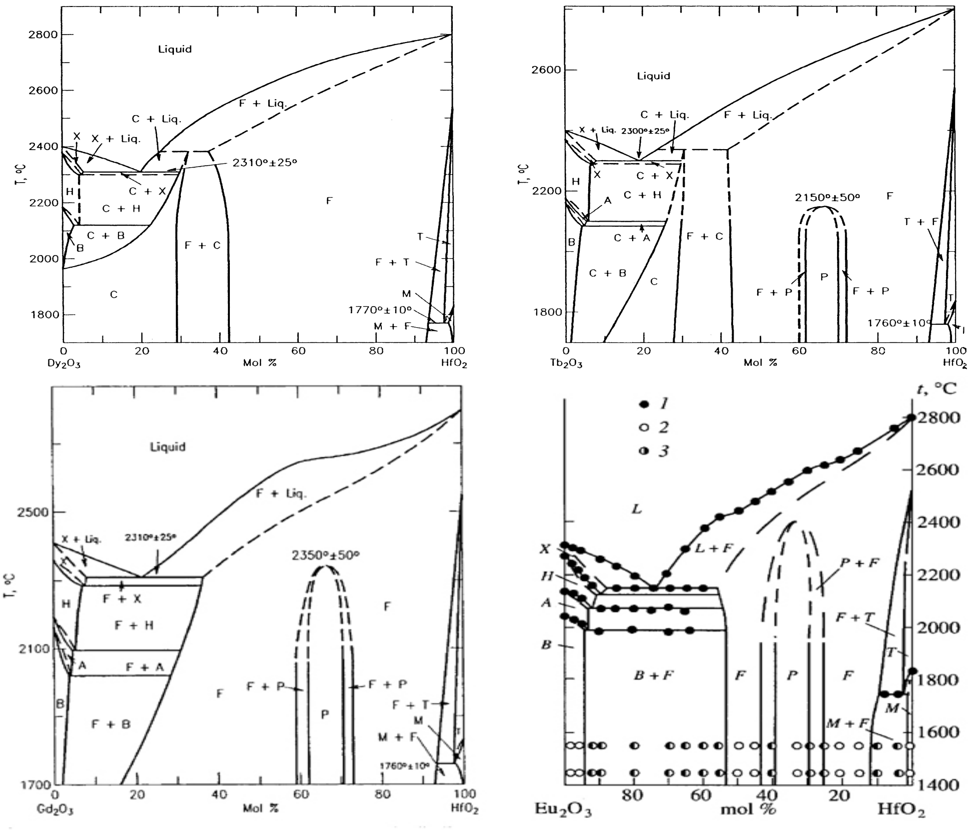

Figure 5.10: Phase diagrams of the $A_2Hf_2O_7$ series of compounds for intermediate A^{3+}, reproduced from [236, 237]. Here the A^{3+} cations have the ionic radii of Dy^{3+} = 1.027Å, Tb^{3+} = 1.04Å, Gd^{3+} = 1.053Å and Eu^{3+} = 1.066Å.

Of particular interest in the hafnate phase diagrams are the larger A^{3+} cations (i.e. Sm^{3+}, Nd^{3+}, Pr^{3+} and La^{3+}, shown in Figure 5.11). In particular, in all of these diagrams the BO_2 excess non-stoichiometry extends to approximately 70 mol percent BO_2. That is, the extent of non-stoichiometry is essentially constant as a function of increasing A cation radius. Conversely, there does seem to be some variation in A_2O_3 excess non-stoichiometry between compounds. This observation will be returned to in Section 5.3.4.

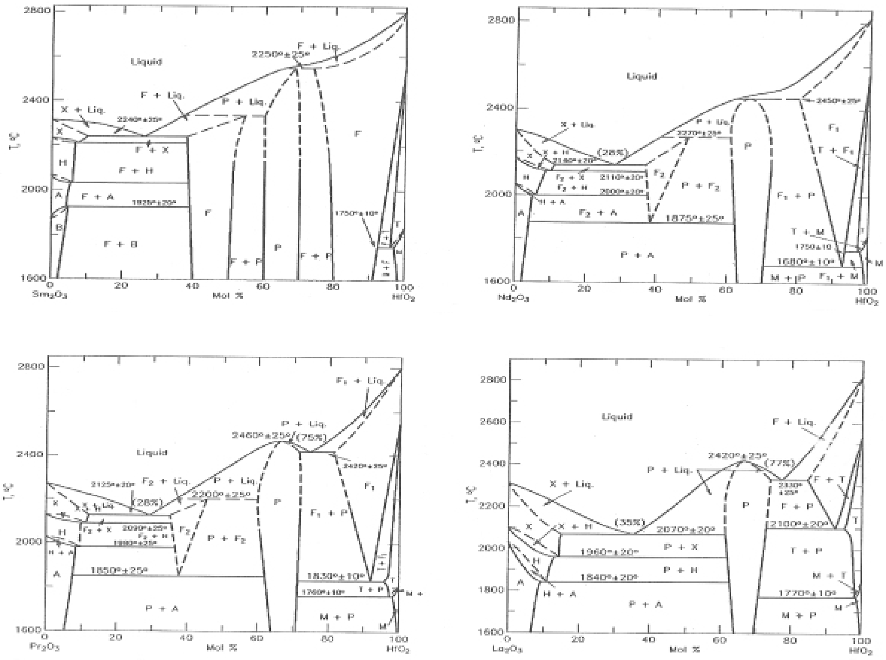

Figure 5.11: Phase diagrams of the $A_2Hf_2O_7$ series of compounds for large A^{3+}, reproduced from [238]. Here the A^{3+} cations have the ionic radii of Sm^{3+} = 1.079Å, Nd^{3+} = 1.109Å, Pr^{3+} = 1.126Å and La^{3+} = 1.16Å.

An advantage of the A_2O_3 - HfO_2 series of phase diagrams is that they were generated by a single research group, thus reducing error which may occur due to inconsistencies in the experimental approaches of different research groups. Of course, this also has its limitations, and it would be desirable to have further verification of the validity of these diagrams.

Finally, phase diagrams for the $A_2Ru_2O_7$, $A_2Mo_2O_7$ or $A_2Sn_2O_7$ series of compounds were unable to be found.

5.1.2 Previous Modelling Studies

There have been a number of previous modelling studies which have focused on specific pyrochlore compounds. In particular, defect formation energies and anion migration in $Gd_2Zr_2O_7$ were studied as a function of doping and disorder by Wilde and Catlow [239, 240]. In addition, Williford *et al.* [241, 242] focused on defect energetics as well as both cation and anion migration as a function of cationic disorder in $Gd_2Ti_2O_7$-$Gd_2Zr_2O_7$ solid solutions. Recently, a systematic study over a wide range of potential pyrochlore compositions was carried out by Minervini *et al.* [243]. That study attempted to correlate the energies for local disorder on both the anion and cation sublattices with the stability of the pyrochlore lattice compared to the corresponding disordered fluorite solid solution. This work was extended by Pirzada *et al.* [244] who considered the activation energy for oxygen migration, again over the same wide range of composition. Minervini *et al.* have also carried out calculations in order to determine the oxygen positional parameter in pyrochlores in an attempt to correlate these values to disorder [245]. However, no previous simulation studies which have considered the detailed mechanisms responsible for non-stoichiometry in pyrochlore compounds are known.

5.2 Methodology

The calculations carried out to determine deviations from stoichiometry are of the same type as described in Chapter 2, that is, atomistic simulations based on a Born like ionic description of the lattice and using the Buckingham short range potential to describe pair interactions, as well as the shell model to account for polarizability. Reaction energies were calculated by summing the appropriate lattice and defect energies. This process is discussed further in the Section 5.3. Many compounds are considered in this study, and as such, contour maps are employed as a convenient means of conveying such large amounts of data.

5.2.1 Contour Maps

In this study, contour maps have been used as a means of interpreting the large number of reaction energies calculated (see Figures 5.13 - 5.15). The maps sort $A_2B_2O_7$ compounds by their cationic radii: increasing A radius along the ordinate and B along the abscissa. Thus each compound occupies a point on the map. Solid points refer to a stable pyrochlore former for which calculations were carried out. Hollow points refer to compounds which have not been observed to form, i.e. exist as disordered fluorites (thus showing where the pyrochlore to fluorite compositional boundary occurs). Here, such compounds were modelled in the pyrochlore structure since this facilitates the construction of a continuous pyrochlore contour map.

For each compound modelled, a defect energy process is calculated and plotting software [246] generates contours of equal energy over the cation radius surface. Cationic radii and reaction energies are converted to a matrix via the Kriging method [247] (using a smoothness value of 0.5). This method is an optimized linear interpolation from which 3D surfaces can be generated. Using this approach, areas of compositional interest (i.e. that have similar process energies as predicted by our methodology) are easily identified. Furthermore, as these plots pertaining to isolated defects use the same scale, the trends are comparable between plots. An advantage of this approach is that predictions of properties can also be made for pyrochlore structures that were not explicitly calculated (e.g. here for hafnates: $A_2Hf_2O_7$; Hf ionic radius = 0.71Å [6]).

Brisse and Knop [248] have shown experimentally that the pyrochlore lattice parameter of lanthanide stannates ($Ln_2Sn_2O_7$) varies smoothly as a function of lanthanide (Ln) ionic radius. Furthermore, Kennedy [249] has shown using neutron diffraction that the oxygen positional parameter of the lanthanide stannate pyrochlores also changes smoothly as a function of lanthanide radius. These types of experiments support the use of contour maps based on cationic radii as an ordering parameter.

5.3 Results and Discussion

5.3.1 Solution Mechanisms

Our first aim is to investigate the mechanisms responsible for non-stoichiometry and then correlate the results with the relative extents to which different compounds can deviate from their stoichiometric $A_2B_2O_7$ compositions. Such processes are controlled by the energetics associated with the solution reactions. Here, results are reported for the three lowest energy reactions that can be responsible for accommodating BO_2 excess and the three reactions that accommodate A_2O_3 excess without the necessity of including electronic disorder. In each case, results are normalized to reflect excess concentration of A or B ions (i.e. the non-stoichiometry). The normalization factors, which appear in front of each reaction below, have been calculated via the mass action approximation [5]. In Kröger-Vink notation [14], these reactions are as follows:

BO_2 excess:

$$\frac{7}{4}\ (BO_2\ +\ \frac{4}{7}A_A{}^x\ \rightarrow\ \frac{3}{7}B_A{}^{\cdot}\ +\ \frac{1}{7}V_A{}'''\ +\ \frac{2}{7}A_2B_2O_7) \tag{5.1}$$

$$\frac{7}{5}\ (BO_2\ +\ \frac{1}{7}B_B{}^x\ +\ \frac{4}{7}A_A{}^x\ \rightarrow\ \frac{4}{7}B_A{}^{\cdot}\ +\ \frac{1}{7}V_B{}''''\ +\ \frac{2}{7}A_2B_2O_7) \tag{5.2}$$

$$\frac{4}{3}\ (BO_2\ +\ \frac{1}{2}A_A{}^x\ \rightarrow\ \frac{1}{2}B_A{}^{\cdot}\ +\ \frac{1}{4}O_i{}''\ +\ \frac{1}{4}A_2B_2O_7) \tag{5.3}$$

A_2O_3 excess:

$$\frac{2}{3}\ (A_2O_3\ +\ B_B{}^x\ +\ \frac{1}{2}O_O{}^x\ \rightarrow\ A_B{}'\ +\ \frac{1}{2}V_O{}^{\cdot\cdot}\ +\ \frac{1}{2}A_2B_2O_7) \tag{5.4}$$

$$\frac{7}{4}\ (\frac{1}{2}A_2O_3\ +\ \frac{3}{7}B_B{}^x\ \rightarrow\ \frac{3}{7}A_B{}'\ +\ \frac{1}{7}A_i{}^{\cdot\cdot\cdot}\ +\ \frac{3}{14}A_2B_2O_7) \tag{5.5}$$

$$\frac{7}{5}\,(\frac{1}{2}A_2O_3 \;+\; \frac{4}{7}\,{B_B}^{x} \;\rightarrow\; \frac{4}{7}\,{A_B}' \;+\; \frac{1}{7}\,{B_i}^{\cdot\cdot\cdot\cdot} \;+\; \frac{3}{14}A_2B_2O_7) \qquad (5.6)$$

(As previously mentioned, non-stoichiometry compensated by a variation of cationic charge state is not considered, since such reactions do not correspond to binary phase diagrams). For each compound, the constituent perfect lattice and individual defect energies were calculated (as described in Chapter 2) in order to construct the appropriate reaction energies from Equations 5.1 - 5.6 above (this required 900 separate calculations for the isolated defects alone). In all reactions, the lowest calculated lattice energies of binary oxides were used, i.e. bixbyite for A_2O_3 and either fluorite or rutile for BO_2. Where applicable, oxygen "split vacancy" defect energies were used (see Figure 5.12) according to the results of Pirzada, *et al.* [244]. This structure differs from the isolated 48f vacancy as an adjacent 48f oxygen will relax considerably towards the unoccupied 8a site. This effectively creates an additional 48f oxygen vacancy, such that there are two oxygen vacancies and an oxygen interstitial. The vacancies are oriented along the <110>. Oxygen interstitial ions were found to occupy 8a sites, as did A and B interstitials.

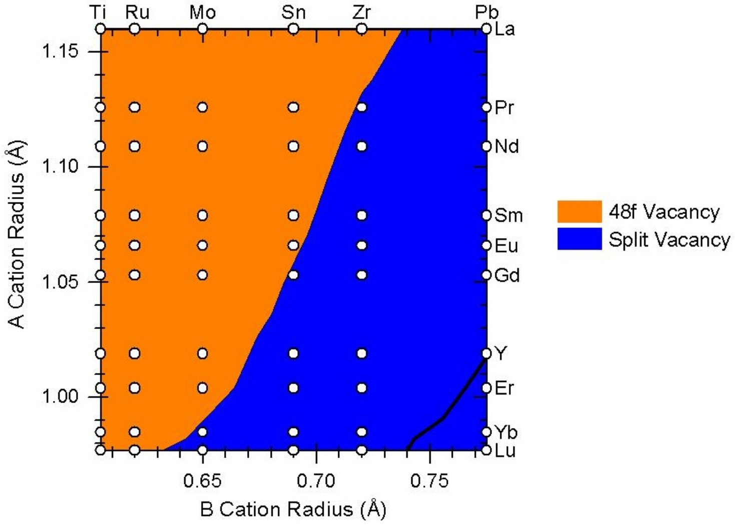

Figure 5.12: Contour map of the energy difference between the split *48f* oxygen vacancy and the split vacancy, where the pyrochlore compounds occurring in the blue region were considered as split and the orange were considered as isolated [244].

5.3.2 Solution at the Dilute Limit

BO_2 Excess

Figure 5.13 shows the results for solution of BO_2 assuming that each defect is isolated. For some compositions, it is evident that there are two competing defect mechanisms for initial BO_2 excess non-stoichiometry. Thus, at small A cation radius and large B cation radius compositions, both A cation vacancies (Reaction 5.1, Figure 5.13a) and oxygen interstitials (Reaction 5.3, Figure 5.13c) will be the compensating defects since both reactions have similar energies. However, when moving toward more stable pyrochlore compositions, the A cation vacancy mechanism becomes considerably more favourable than the oxygen interstitial mechanism. For all compositions, Reaction 5.2 (Figure 5.13b), which involves B cation vacancy compensation, was found to be unfavourable.

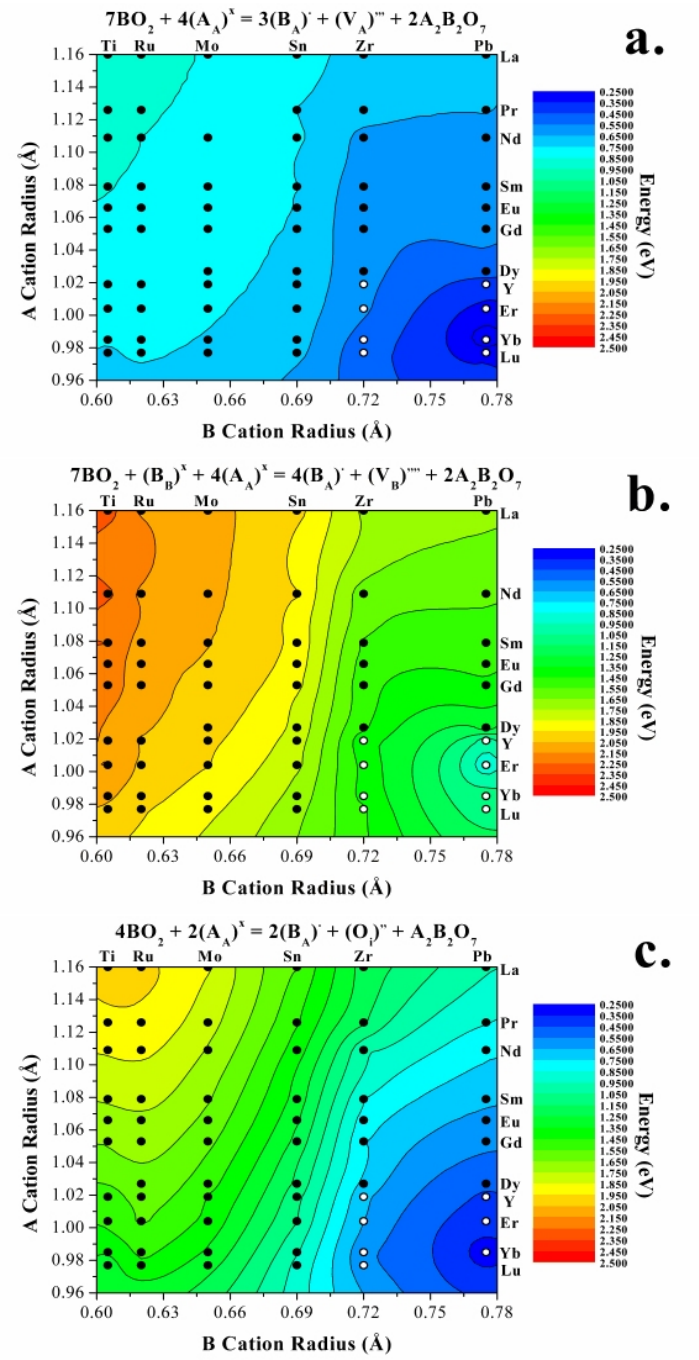

Figure 5.13: Normalized energies for the three mechanisms of BO_2 accommodation in pyrochlore oxides assuming an isolated defect model. Maps a., b. and c. refer to Equations 5.1, 5.2 and 5.3 respectively.

If the pyrochlore structure is considered to be an ordered fluorite solid solution, it seems intuitive that B cation excess should be accommodated by oxygen interstitials. For many compositions, our results are therefore at odds with intuition. Thus, our model implies that non-stoichiometry associated with B cation excess in the most stable pyrochlore compounds (i.e. the majority) is distinct from solid solution formation in fluorites. Consequently, if subsequent experiments show these results to be correct, simply assuming that pyrochlore materials are ordered fluorite solid solutions can be seriously misleading.

B cation non-stoichiometry is therefore an example of how the properties of pyrochlore compounds are predicted to evolve as their compositions move towards the pyrochlore - fluorite stability threshold, described in reference [243]. Another example is the structure of the oxygen vacancy which changes from a symmetric geometry to a split vacancy [244]. However, the boundary for that property occurs somewhat before the pyrochlore - fluorite boundary is reached. It has also been found that the extent of lattice disorder increases dramatically as this boundary is approached [245]. Such disorder demonstrates how the pyrochlore lattice evolves as a function of composition to become more similar to fluorite solid solution. However, this change is not continuous as a function of composition as evidenced by either clear order-disorder transformations (see in particular reference [237]), or by the distinct pyrochlore phase fields (see reference [238]).

Another important feature of the contour plots is how solution energies change as a function of the radii of the constituent ions. For example, in Figure 5.13a, it is clear for stannates, and by extrapolation for hafnates, that the solution energies do not vary greatly as a function of A cation radius, spanning only two contours (this example will be returned to later). Within the titanates, there is modest variation, as three contours are crossed. Conversely, there is a more considerable increase in solution energy when the A cation (e.g. Gd) is kept constant while the B cation radius varies; typically five contours are spanned. This implies that titanate compounds have significantly higher solution energies than zirconates or hafnates.

A_2O_3 Excess

From Figure 5.14, it is clear that initial A_2O_3 excess will always be compensated by oxygen vacancies (i.e. Equation 5.4, Figure 5.14a). Therefore, non-stoichiometry associated with A_2O_3 excess is simpler than BO_2 excess in that a single solution mechanism is dominant over the entire compositional range considered. In this regard, the pyrochlore lattice is behaving like a fluorite lattice since it is well established that fluorites also accommodate the solution of A^{3+} cations by forming oxygen vacancies [250].

From Figure 5.14 it is also apparent that, for corresponding compounds, the accommodation of A_2O_3 is a higher energy process than BO_2 accommodation. This should imply that the extent of A_2O_3 solution will be lower than that of BO_2. However, the energies predicted for the hafnate series, for example, indicate that there will be considerable solution of A_2O_3 (despite the fact that our over-estimation of energies via the full charge model will tend to underestimate the extent of solution). As a consequence, it is not complete to rely only on an isolated defect model to understand the extent of solution. Therefore, defect cluster formation must be modelled.

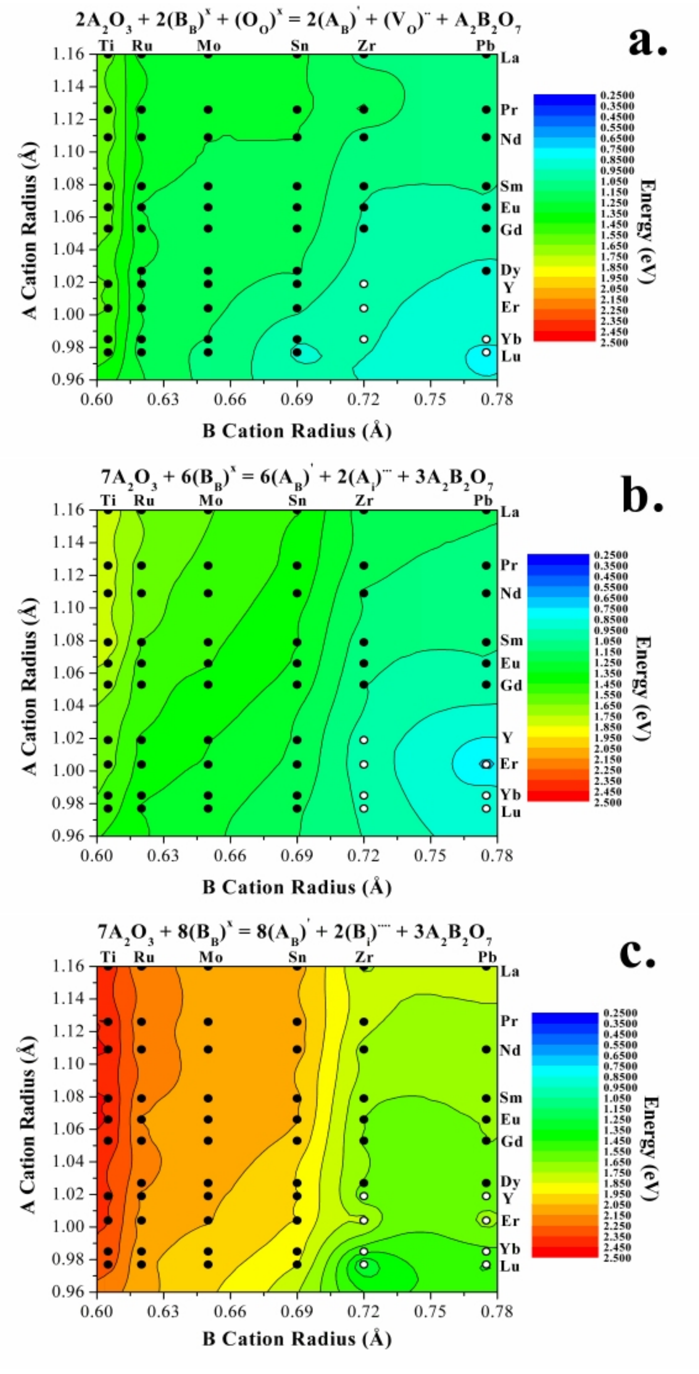

Figure 5.14: Normalized energies for the three mechanisms of A_2O_3 accommodation in pyrochlore oxides. Maps a., b. and c. refer to Equations 5.4, 5.5 and 5.6 respectively.

Finally, for A_2O_3 excess, the distribution of solution energies can be considered as a function of composition (as was the case for BO_2 excess). The most favourable mechanism, i.e. Equation 5.4, Figure 5.14a, shows that the titanate series exhibit substantially higher solution energies than do zirconates, hafnates or stannates. This is similar to BO_2 excess. However, there are differences compared to BO_2 excess when the change in energies is considered within a B cation series as a function of varying A cation radius. In this case for the titanates and ruthanantes, no contours are crossed, i.e. there is no A cation radius dependence. Whereas for the zirconates, stannates and hafnates, the energy range extends over four contours, i.e. there is considerable A cation radius dependence.

5.3.3 Effect of Defect Clustering

For each defect cluster considered, it is initially necessary to ascertain its minimum energy configuration. This becomes challenging with the increasing number of constituent defects per cluster and the complexity of the lattice. Regardless, the preferential geometries for the three low energy mechanisms (i.e. Equations 2 and 4 for BO_2 solution and Equation 5 for A_2O_3 solution) were determined. The geometries are available in Table 5.1 and were used for all cluster calculations.

Defect Cluster Constituent	x	y	z
Reaction 2			
$(\mathrm{B}_A)^{\cdot}$	0.5	0.0	0.0
$(\mathrm{B}_A)^{\cdot}$	0.5	0.5	0.5
$(\mathrm{B}_A)^{\cdot}$	0.25	0.25	0.5
$(\mathrm{V}_A)'''$	0.5	0.25	0.25
Reaction 4			
$(\mathrm{B}_A)^{\cdot}$	0.5	0.0	0.0
$(\mathrm{B}_A)^{\cdot}$	0.0	0.5	0.0
$(\mathrm{O}_i)''$	0.125	0.125	0.125
Reaction 5			
$(\mathrm{V}_O)^{\cdot\cdot}$	0.330	0.125	0.125
$(\mathrm{A}_B)'$	0.25	0.25	0.0
$(\mathrm{A}_B)'$	0.0	0.25	0.25

Table 5.1: The perfect lattice coordinates for the preferential configuration of compensating defect clusters.

If the solution of BO_2 is considered first (see Figures 5.15a and 5.15b, where the solution energies for Equations 5.1 and 5.3 are presented), it is evident that clustering of the compensating defects lowers the overall energy (compare to Figures 5.13a and 5.13c). It is also evident that for all stannates and hafnates (Hf ionic radius = 0.71Å [6]), the solution of BO_2 is still largely independent of A cation radius (i.e. the range of solution energies is no greater than 0.2eV over these series). However, the situation for the titanates is once again more complex with solution energies increasing as a function of A cation radius (the variation is 0.7eV over the titanate series).

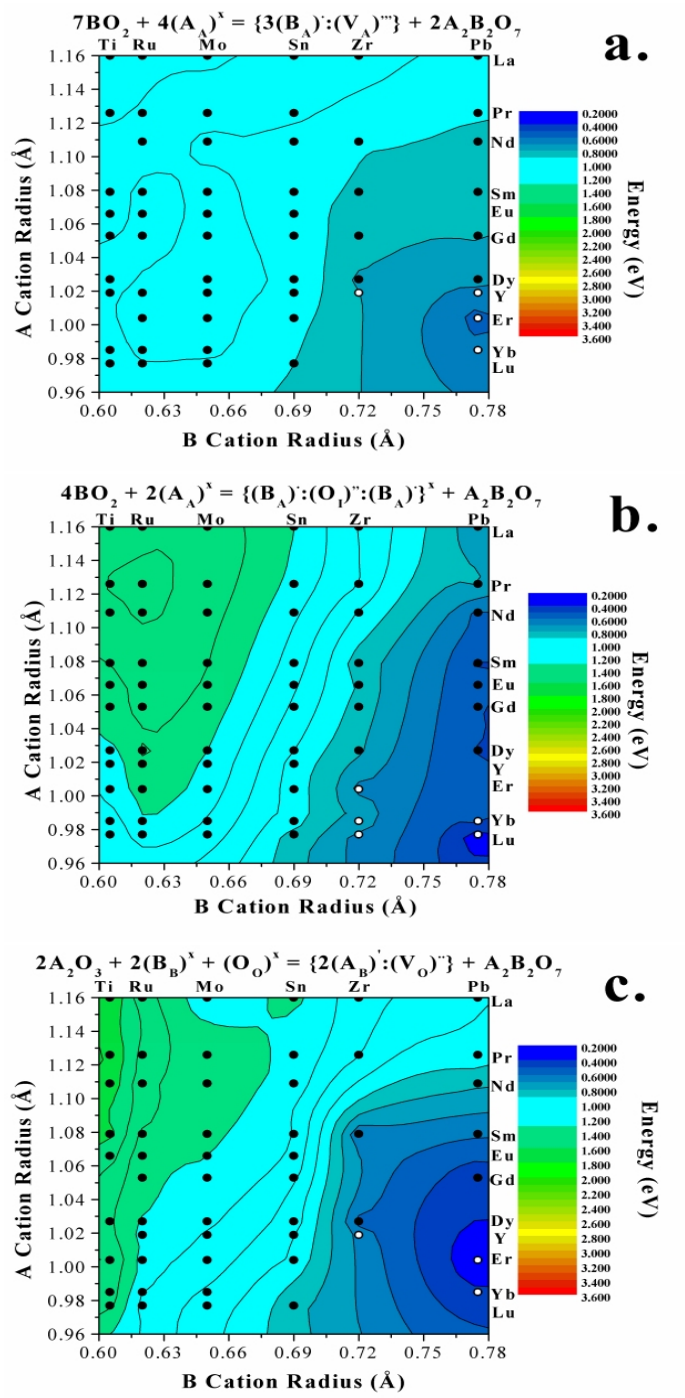

Figure 5.15: Solution energies for the three low energy solution mechanisms calculated assuming clustered defects. Maps a., b. and c. refer to Equations 5.1, 5.3 and 5.6 respectively.

Although defect clustering lowers reaction energies, the distribution of contour positions remains similar (compare values in Figures 5.13a, 5.13c and 5.14a with Figures 5.15a, 5.15b and 5.15c respectively). For example, Figure 5.13c shows a dip in the bottom left corner as does the corresponding Figure 5.15b. Nevertheless, the spacing between contours is greater in Figure 5.15 since clustering leads to smaller variations in solution energies between compounds (with the same energy scale used for all diagrams). However, clustering does not change the lowest predicted energy mechanisms for accommodation of non-stoichiometry deduced from the results assuming an isolated defect model.

5.3.4 Comparison to Phase Diagrams

The results presented in sections 3.2 and 3.3 above can be correlated to the phase diagrams which include the $A_2Ti_2O_7$, $A_2Zr_2O_7$ and $A_2Hf_2O_7$ compounds.

This comparison begins by considering the most complete set of phase diagrams, that is, those diagrams that exhibit a stable $A_2Hf_2O_7$ compound [235–238]. These diagrams show that the extent of BO_2 excess non-stoichiometry is not drastically affected by varying the A cation radius (the stoichiometry range limit is approximately constant at 70 mol percent BO_2). This behaviour is consistent with the prediction of Figures 5.13a and 5.15a, in that only one contour is crossed, i.e. the solution energy does not alter greatly with varying A cation. The low energies in this region of the map are also consistent with the considerable BO_2 excess non-stoichiometry observed experimentally.

Considerable A_2O_3 excess non-stoichiometry is also predicted in the hafnates, as a consequence of the low energy regions of the contour maps Figures 5.14a and 5.15c. This is also in qualitative agreement with experimental observations. For $A_2Hf_2O_7$, where A = Sm, Eu and Gd, the solution energy for A_2O_3 excess is practically the same as for BO_2 excess. Thus the pyrochlore phase field should be essentially symmetric about the stoichiometric ratio (i.e. at $\approx 66\frac{2}{3}$ mol percent BO_2). Again, this is what is observed [237]. However, the energies for A_2O_3 excess begin to increase for compounds of larger A radii, e.g. Nd, Pr and La. From this prediction, a reduction in the extent of A_2O_3 excess non-stoichiometry is expected for these compounds. Although, it is difficult from the experimental data to be definitive, as the A radius increases, the extent of A_2O_3 excess non-stoichiometry does indeed seem to fall from approximately 60 mol percent BO_2 to approximately 64 mol percent BO_2 [238].

Many titanate phase diagrams [214–218] have the pyrochlore structure occurring only as a line compound, recall Figure 5.1. Conversely, several phase diagrams mentioned contradict this picture and show a deviation from pyrochlore stoichiometry which is pronounced in the BO_2 direction but still non-existent in the A_2O_3 direction see Figures 5.2 and 5.3 [221, 222]. Our results do predict that the titanates will exhibit less deviation from stoichiometry than will other series of B cations. However, for BO_2 excess, since these solution energies for the titanates are only modestly greater then for zirconates or hafnates (see Figure 5.15a), some discernable deviations from the stoichiometric ratio for BO_2 excess is expected. Conversely, little if any non-stoichiometry is expected for A_2O_3 excess, due to the rather high relative energy of this process (see Figures 5.14a and 5.15c).

A contributing factor to difficulties in investigating the titantates experimentally compared to the hafnates might be the greater difference between the solution energies predicted assuming isolated defects (Figure 5.13a) versus clustered defects (Figure 5.15a). Since cluster formation in titanates lowers solution energies more, it may be that titanates take longer to reach equilibrium than do hafnates as cluster formation requires cation migration. Nevertheless, it would seem to be potentially worthwhile to revisit the titanates experimentally.

It is difficult to make any definite comparisons to the existing set of zirconate phase diagrams [223–226], due to the predominantly hypothesized nature of their pyrochlore phase fields. However, what is clear from these phase diagrams is that the zirconate pyrochlores are expected to exhibit non-stoichiometry in both the BO_2 and A_2O_3 directions. The relative energies observed in the contour plots predict slightly greater deviations from stoichiometry for the zirconates than for the hafnates. Again, the phase fields should be essentially symmetric for $A_2Zr_2O_7$ where A = Dy to Sm, but asymmetric with greater ZrO_2 excess than A_2O_3 excess for A = Nd to La.

Of course, it is desirable to have a more complete series of phase diagrams with which to compare the current predicted trends. Hopefully, this study will stimulate further experimental work focused on determining the extent of non-stoichiometry in various pyrochlore oxides. Given the excellent crystallographic data available for the stannates [249, 251] and their significant non-stoichiometry, this series may be particularly profitable to study.

5.4 Conclusions

There are a number of general and specific conclusions that result from this work. Firstly, some general comments are made.

Given the great number of calculations necessary to carry out this comparative type study, a simple computational approach was employed. Given the limitations of such a methodology, trends have been focused on, rather than absolute solution energies. However, the trends are clearly complex and therefore required a contour map approach to aid with interpretation.

It seems that the calculated trends agree with the available, albeit confused, experimental data. The maps can therefore be used as a basis for further systematic experimental studies. Furthermore, the maps can be used to select compositions that exhibit greater or lesser deviations from stoichiometry. Of course the maps can be used predictively to consider elements which have not been explicitly modelled, but whose ionic radii are known. This may also include certain compounds whose elements that are able to exhibit variable charge states (e.g. Pr and Ce containing). This will form the basis of a future study.

Some specific comments should also be made.

- It is predicted that for stable pyrochlore formers, non-stoichiometry associated with BO_2 excess is generally accommodated by forming A^{3+} cation vacancies. As the pyrochlore - fluorite boundary is approached, oxygen interstitial ions will also contribute to the solution mechanism, resulting in complex defect behaviour.

- These calculations therefore demonstrate that the mechanism for BO_2 excess non-stoichiometry in pyrochlore oxides is distinct from solid solution formation in fluorite, especially for the majority, stable pyrochlore compositions.

- Oxygen vacancies are clearly the defects that accommodate the solution of excess A_2O_3 in all pyrochlore compositions considered in this study. In this regard, pyrochlores are behaving like fluorite solid solutions.

- The clustering of compensating defects lowers the overall energy of each mechanism, but does not affect the preferential solution mechanism or greatly affect the relative energies predicted by isolated defect calculations.

- The model predicts that the extent of BO_2 excess non-stoichiometry in hafnates, zirconates and stannates will be considerably greater than for titanates or ruthanates. Furthermore, while the possible deviation is constant for hafnates in particular, it decreases as a function of increasing A cation radius for the titanates.

- Similarly, the extent of A_2O_3 excess non-stoichiometry in hafnates, zirconates and stannates is again much greater than for titanates or ruthanates, the latter probably not exhibiting any substantial deviation.